Chapter 3
Development of Coal Roof Index (CRI)

3.1 General

As discussed in Chapter 2, existing rock mass classification systems such as *RMR*, Q-system, *CMRR*, and *CMRI-RMR* have been successfully applied in various underground mining environments. However, for Indian coal mines, these systems often show limitations in predicting stand-up time accurately, particularly for short-term stable roofs. The influence of individual weak parameters, as well as the combined effects of gallery dimensions and in-situ stress conditions, is not fully captured in existing approaches. The stability of an unsupported coal mine roof depends on several interrelated factors, including: roof strata quality (as determined by geotechnical classification), gallery span and geometry, and in-situ stress conditions. These factors collectively determine the stand-up time, which is a key parameter for assessing roof stability and designing safe and economic support systems.

It has been observed, particularly for the short-term stable cases (i.e., less than 30 days), that the *CMRI-RMR* value has a wide range from 27 to 62, which shows a poor correlation between stand-up time and *RMR* values. After a re-look at these cases, it was observed that the rating of the single parameters is low compared to other parameters for most of the cases. This indicates that the influence of a single weak parameter is sufficient enough to reduce the strength of the roof mass. Therefore, the summation of the ratings for estimation of the overall rating of the rock mass is not appropriate. A correlation graph between the stand-up time and *CMRI-RMR* has been plotted in Fig. 3.1.

To address the shortcomings of existing classifications, a new geotechnical classification system, the *CRI*, is proposed in this study. The *CRI* is designed to better

reflect the multiplicative effect of critical parameters and to incorporate stress–dimension adjustments through a *RLF*. The development of the *CRI* is based on the analysis of 44 cases from Indian coalfields, as documented in scientific and technical reports (CMRI Report, 1987). These cases represent a wide range of geological, geotechnical, and mining conditions, enabling a robust evaluation of the relationship between stand-up time, roof quality, and other influencing factors.

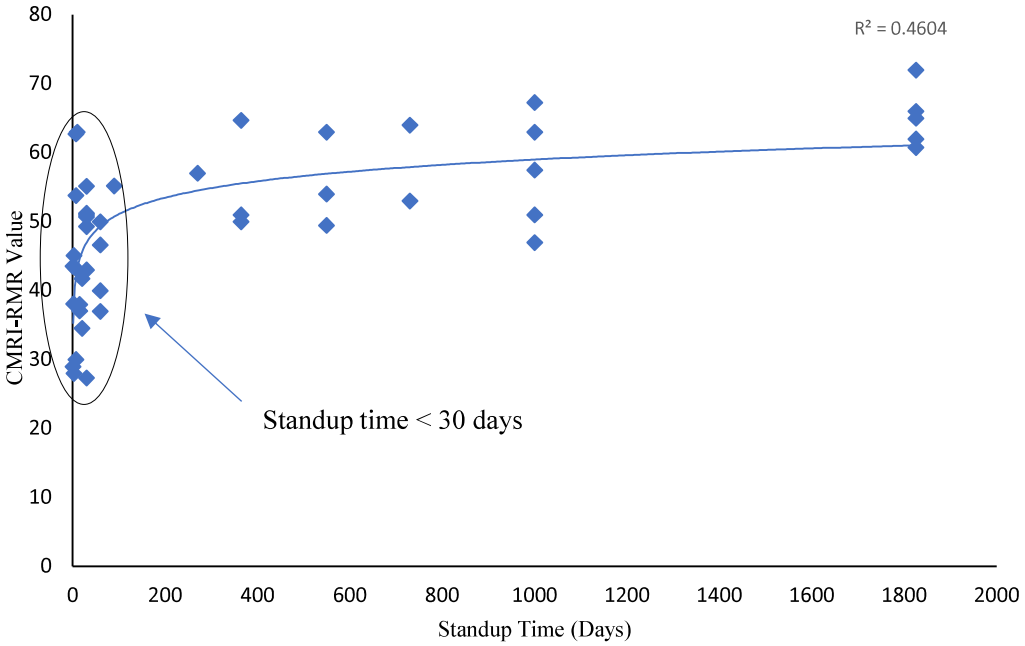

Fig. 3.1: Correlation between recorded stand-up time and calculated *CMRI-RMR.*

3.2 Case Study

Forty-four Indian underground coal mines were considered for the development of geo-mechanical classification. The database consists of 9 immediately failed cases (standup-time < 7 days), 16 short-term stable (7 days <stand-up time <90 days), and 19 long-term stable cases, as shown in Table 3.6. The depth and width of the gallery vary from 20 m to 400 m and from 3.0 m to 4.8 m, respectively. The geo-mechanical parameters for all 44 cases are given in Table 3.1 (*CMRI* Report, 1987).

Table 3.1: Data set for 44 Indian coal mines (*CMRI* Report, 1987).

Sr. No.	Colliery Name	Depth (m)	*ST* (Days)	*LTH* (cm)	*SF*	*SDI* (%)	*UCS* (*MPa*)	*Gw* (ml/min)	Adj. *RMR*	Adj. *CRI*
1	Lachipur	220	30	4.10	6	50.00	22.40	9	51.20	1.81
2	Bahula	96	3	6.50	15	90.00	8.10	175	45.10	1.67
3	Jambad	71	15	2.00	7	67.70	50.00	100	38.00	5.36
4	Jamdoba	386	30	4.50	11	98.80	29.50	10	45.90	12.57
5	Lalmatia	30	1	3.00	11	95.03	3.50	500	28.96	1.33
6	Jarangdih	20	7	4.00	9	95.00	22.50	1.2	62.75	3.71
7	Venkatesh Khani	173	2	2.61	13	93.84	16.74	10	38.10	1.13
8	Khas Kajora	330	30	5.00	7	99.50	24.00	9	45.62	23.58
9	Lohapatti	30	3	3.20	15	68.00	24.90	9	28.00	1.06
10	Bhelatand	310	20	3.10	9	99.02	21.73	2500	37.58	5.03
11	Chhapapur	80	30	4.16	8	98.76	27.00	175	49.30	20.96
12	Seetalpur	390	7	3.20	9	98.70	17.00	1.2	53.80	4.06
13	Mithapur	42	30	11.00	17	94.12	28.00	9	43.00	11.50
14	Newton Chickli	225	30	2.91	12	95.80	14.02	12	27.36	2.60
15	Rakhikol	275	7	3.23	14	98.65	21.25	210	27.00	3.77
16	Sukri	225	20	2.49	13	99.06	28.78	100	34.57	4.02
17	Kuju	30	30	5.50	9	98.80	20.93	1.2	55.16	13.41
18	Jhanjra	18	1	3.76	9	83.75	34.07	200	43.54	4.76
19	Madhuband	150	15	2.50	10	94.03	63.00	1.2	37.10	15.63
20	Sripur	335	7	3.85	11	94.18	33.74	5	38.88	8.93
21	Topa	20	730	5.00	12	98.90	55.00	9	53.00	36.11
22	Goutam Khani	200	1825	15.00	6	98.50	59.00	1.2	62.00	127.45
23	Chora	150	1825	12.00	4	94.95	38.82	9	66.00	145.09
24	Visesher Khandra	84	1825	5.90	5	97.33	22.03	1.2	60.75	47.15
25	New Kenda	28	1825	9.00	3	99.00	35.00	1.2	72.00	162.50
26	Kharkharee	160	270	6.50	8	96.63	51.00	9	57.00	95.21
27	Kuardih	137	1000	4.63	3	98.96	43.44	1.2	67.27	97.94
28	Amritnagar	75	365	9.16	4	98.59	20.96	1.2	64.70	99.02
29	Jaykay Nagar, Bogra	112.5	730	7.00	4	98.00	31.80	1.2	64.00	108.82
30	Jaykay Nagar, Satgram	141	550	5.50	6	94.76	25.80	9	54.00	18.14
31	Barmondia	190	550	4.78	9	97.13	28.30	9	49.45	19.35
32	Ningah	400	1825	5.60	4	98.00	53.20	1.2	65.00	120.50
33	Jamehari	92	1000	7.50	3	96.27	26.00	9	63.00	75.45
34	Kuya	145	1000	5.00	10	97.00	35.00	70	47.00	19.35
35	Bastacolla	92	1000	5.60	8	96.80	28.66	24	51.00	23.58
36	Dobari	80	1000	4.25	6	98.55	33.35	1.2	57.50	38.69
37	Bankola	105	365	4.39	8	93.40	30.21	1.2	51.00	27.90
38	East Katras	54	550	10.70	4	91.85	25.00	1.2	63.00	100.60
39	Chapui Khas	225	365	3.28	7	95.93	20.77	1.2	50.00	14.15
40	Muruldih	180	60	3.00	15	97.86	20.60	9	37.00	3.23
41	Sudamdih	300	60	8.50	12	88.90	49.00	9	45.00	15.19
42	Kedla	60	90	8.18	12	99.04	33.50	9	55.20	24.38
43	Rawanwara	200	60	2.00	12	97.78	21.00	15	40.00	4.53
44	East Dongar Chickli	300	60	4.02	11	96.31	21.82	1.2	41.96	12.57

Here, *ST*= Stand-up time (days), *LTH* = Layer thickness (cm), *SF* = Structural Features, *SDI* = Slake durability index, *UCS* = Uniaxial Compressive Strength (*MPa*), *Gw* = Ground water flow (ml/min)

3.3 Coal Roof Index

Keeping above fundamental issue, particularly related to poor rock quality, a new *CRI* classification system has been proposed. The proposed classification system is based on the multiplication of individual dependent parameters' rating, similar to the Q-system of rock mass classification as given below:

$$CRI = \left(\frac{R_{CRI\_1}}{R_{CRI\_2}}\right) X \left(\frac{R_{CRI\_3}}{R_{CRI\_4}}\right) X R_{CRI\_5} \quad (3.1)$$

But as various researchers have shown, the depth, width, and height of the gallery also play an important role in the stability of the coal gallery. It is directly affected to the unsupported span, excavation cycle, and support design. Therefore, the author has introduced the '*RLF*' for the combined effect of the dimensions of the gallery and stress conditions. The calculation of *RLF* has been discussed in Section 3.3.6. The adjusted *CRI* has been determined by the division of *CRI* to the rating of six parameters (*RLF*) as follows:

$$\text{Adjusted } CRI = \frac{CRI}{R_{CRI\_6}} \quad (3.2)$$

$$\text{Adjusted } CRI = \left(\frac{R_{CRI\_1}}{R_{CRI\_2}}\right) X \left(\frac{R_{CRI\_3}}{R_{CRI\_4}}\right) X \frac{R_{CRI\_5}}{R_{CRI\_6}}$$

The *CRI* ratings for *LTH*, SF, weatherability, *Gw*, *UCS* of roof strata, and *RLF* are denoted by the letters R_{CRI_1}, R_{CRI_2}, R_{CRI_3}, R_{CRI_4}, R_{CRI_5}, and R_{CRI_6}. When dealing with multiple layers along with the bolted zone, or roughly 2.5 m, the weighted average value of the *CRI* can be calculated.

3.4 Determinations of parameter values

3.4.1 *LTH* measurement

LTH is a very important parameter for understanding the roof behaviour as it is related to the delamination of the strata, a principal causative factor for deterioration of roof condition. Whereas the thickness of noticeable lamination or layers is assessed for shale roofs, the thickness of bedding planes per meter is measured for sandstone roofs. In contrast, when it comes to a coal roof, the thickness of noticeable bands is measured. The *LTH* can be represented indirectly by *RQD* (Priest and Hudson, 1976) expressed as:

$$RQD=100\ (0.1\lambda+1)\ e^{-0.1\lambda} \qquad (3.3)$$

Where λ = frequency of bedding planes

LTH can be estimated by the inverse of the frequency of bedding planes. The average of the disposition measurement of different layers is a common method of determining the *LTH* of the immediate roof (Fig. 3.2). *LTH* can also be determined by borehole camera, such as slim borehole scanner, after drilling hole in the immediate roof, in case layers in the roof are not visible.

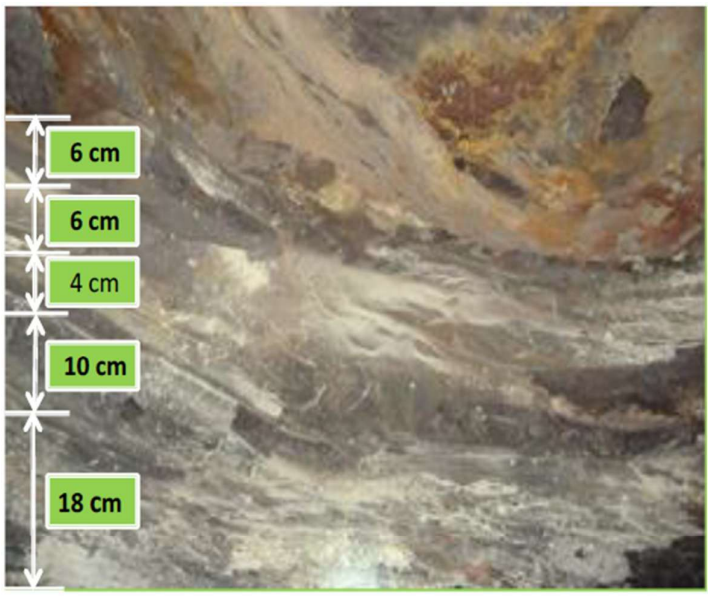

Fig. 3.2: Determination of *LTH* in coal mine roof (Paul, 2020)

LTH can also be determined by a borehole camera, such as a slim borehole scanner, after drilling a hole in the immediate roof, in case layers in the roof are not visible.

3.4.2 Structural Feature

SF include joints, cleats, fractures, slips, slickensides, faults, and folds. Other sedimentary features like Clastic dyke, Kettle bottoms, Ball coal, etc., are also responsible for strata control problems. Joints, fractures, and cleats are structural discontinuities in rock strata that result from brittle deformation. They are planar discontinuities with no displacement parallel to the plane of the fracture, joint, or cleat face. Joints occur as families of fractures displaying similar orientation, spacing, and extent in a given rock type, whereas fractures occur singly. Cleats are analogous to joint systems occurring in coal. The existence of such features results in unstable roof conditions. Roof stability is influenced by how mine workings are oriented in relation to the joint system. Fractures/joints oriented parallel to the main entries of the coal mine are often unsupported by coal pillars and contribute to unstable ground conditions. According to Smith (1992), the most adverse orientation of a prominent cleat system (face cleats) is when it dips vertically with the strike parallel to the pillar walls.

Table 3.2: Indices for the Parameter 'SF' (Venkateswarlu et al., 1989)

i. Major faults cutting across the gallery

Net slip> 10m	slip 2-10 m	slip < 1 m
15	8	5

ii. Presence of minor faults/slips

spacing < 5m		spacing >5 m	
Orientation unfavourable	Orientation not unfavourable	Orientation unfavourable	Orientation not unfavourable
10	5	7	3

iii. Occurrence of slickensides in the roof

spacing < 10 cm		spacing> 10 cm	
1-3 mm opening	Apparently tight	1-3 mm opening	Apparently tight
8	6	6	4

iv. Occurrence of joints and cleats

a) Minimum spacing < 30 cm

	2-5 mm opening		*0-2 mm opening*	
	orientation unfavourable	Orientation not unfavourable	orientation unfavourable	Orientation not unfavourable
Single set	6	4	5	3
Two set	7	6	6	4
> 2 sets	8			

b) Minimum spacing> 30 cm

	2-5 mm opening		*0-2 mm opening*	
	orientation unfavourable	Orientation not unfavourable	orientation unfavourable	Orientation not unfavourable
Single set	5	2	4	1
Two set	6	4	5	3
> 2 sets	6			

Index for 'SF' = sum of indices for individual features

3.4.3 *SDI*

Weathering causes coal measure rocks to weaken or crumble, particularly when water is present. Slake durability indicates susceptibility to weathering. The *SDI* is measured by the slake durability apparatus as per the International Society for Rock Mechanics (*ISRM*) standard, which is shown in Fig. 3.3.

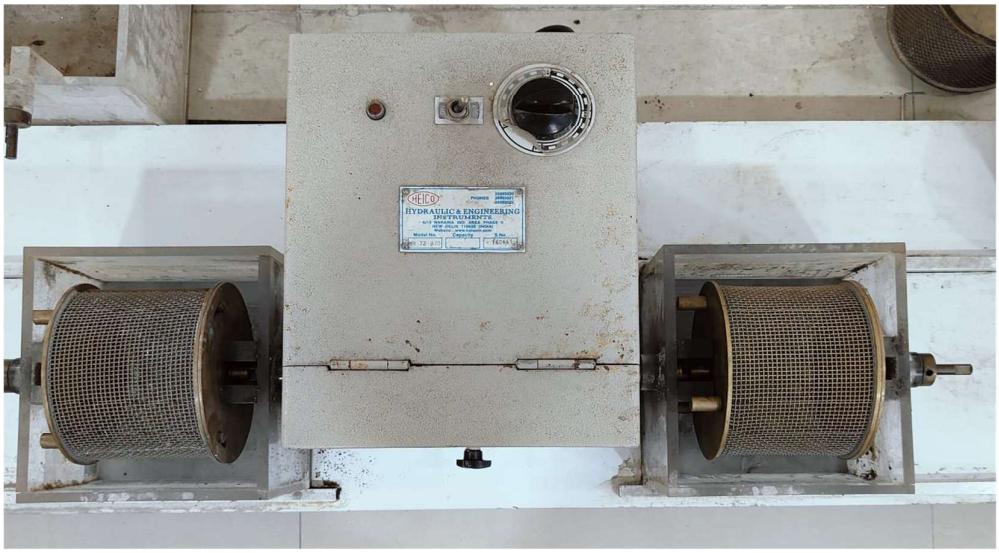

Fig. 3.3: Slake durability testing apparatus

Ten nearly equal-sized, spherically shaped pieces of fractured rock, each weighing between 40 and 60 grams, are taken, for a total sample weight of around 500 grams. The test drum is filled with the samples. For ten minutes, the drum is rotated at 20 rpm while partially or completely submerged in water. Less than 2 mm of shattered material will be able to flow through the drum's mesh. Following the initial 10-minute cycle, the drums are placed in an oven set to 1100° C for approximately 6 hours to dry the samples before being weighed. The first cycle *SDI* is calculated as the weight percentage of material retained in the drum. The purpose of the slake durability test is to evaluate the sample's resistance to weakening and disintegration after it has been put through a typical cycle of drying and wetting in a slaking fluid, often water. The following formula determines the I^{st} Cycle *SDI* (ISRM, 1977):

$$SDI = [(B - D / A - D) \times 100] \quad (3.4)$$

where A represents the combined weight of the drum and sample, B represents the combined weight of the drum and the portion of the sample retained after the test, and D represents the weight of the cleaned drum.

3.4.4 *UCS*

The universal testing machine (*UTM*) is used to determine the compressive strength of the rock in the laboratory using either borehole cores or one-inch cubes prepared from a larger block of rock cut from the mine roof. The specimen's sides are smoothed off, and its ends are made flat to prevent any sudden abnormalities. The specific sample dimensions and a length-to-diameter ratio (*L/D*) should be 2.5-3.0. An error of 0.01mm in the length, breadth, and height of the specimen is permissible. The specimen is continually loaded at a steady stress rate, causing failure 5–10 minutes after loading (Fig. 3.4). According to *ISRM* standards (1964), the stress rate falls between 0.5 and 1.0 MPa per second. The highest load that the rock specimen can support is divided by the initial cross-sectional area to determine its *UCS*.

Fig. 3.4: UCS Testing Machine

$\sigma_c = [F/A]$ (3.5)

where A is the cross-sectional area (cm2), *F* is the failure load in kg, and *σc* is the *UCS* in kg/cm2.

3.4.5 Ground Water Condition

A 1.5–2 m hole is drilled in the roof, and the water that percolates through it is collected to measure groundwater seepage. After a minute of collecting the water in a beaker, the volume is measured in millilitres. As a result, ml/min is used to indicate the water percolation rate. The occurrence of groundwater is problematic, especially when shales and clays are found frequently interbedded with coal seams in the roof rocks (Venkateswarlu et al., 1989).

3.4.6 *RLF*

Previous studies have demonstrated that the depth, width, and height of a coal gallery significantly influence its stability. These parameters directly affect the unsupported span, excavation cycle, and support design. To quantify the combined influence of gallery dimensions and stress conditions, this study introduces the *RLF* as an input parameter in the *CRI*. Therefore, a numerical exercise has been done considering the average rock mass conditions.

In Indian coal mines, the depth and width of underground openings vary from 20 m to 300 m and 3.0 m to 6.0 m, respectively. Therefore, the author has chosen seven various depths for numerical modelling as 50 m, 100 m, 150 m, 200 m, 250 m, 300 m, and 350 m, and the width of galleries chosen as 3.0 m, 4.0 m, and 5.0 m. The height of the gallery has been considered as 3.0 m and 4.0 m. The phase 2D tool has been used for numerical analysis of the effect of depth and width on the roof stability. The stress distribution around the gallery has been studied for various permutations and combinations of cases. The roof fall height was observed as the height of the yielding

zone from the roof edge of the gallery for each combination. The statistical analysis has been done considering the observed *RLH* from the numerical method. The author has developed a relationship for *RLF*, which is incorporated in the *CRI* as an input parameter.

Fig. 3.5 has been included to illustrate the finite element mesh and boundary conditions used in the numerical modelling of a 4.0 m wide underground gallery. The left panel shows the full model domain, while the right panel provides a zoomed-in view of the gallery section, highlighting the three considered span widths.

Table 3.3: Material properties used in numerical modeling

Rock mass properties for roof and floor	Young's modulus	Poission ratio	*m*	*s*	*a*
Value	5 GPa	0.3	1.2	0.016	0.5

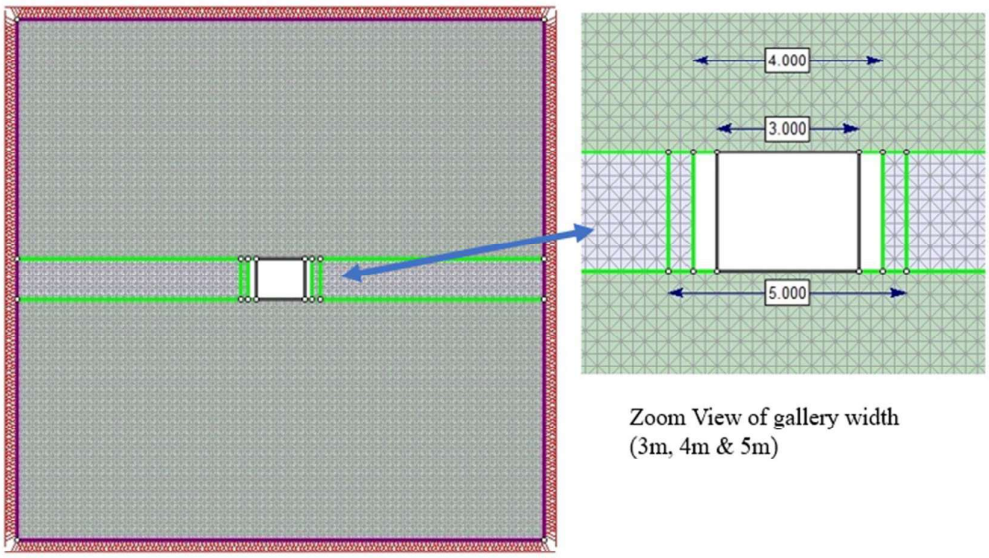

Fig. 3.5: Numerical model of 4.0 m wide gallery

The H-B failure criteria have been considered. The material properties assessed from resembling the Shoery equation (Eq. 2.9 to 2.11) for the average *RMR* value of 50. The deduced values of the strength parameter (m and s) are tabulated in Table 3.3, with a

value of 0.5 considered. It is presumed that the plot of *RLH* for other values also follows a similar trend.

Numerous writers have tried to properly initialize pre-mining stress in intricate situations (S. Kumar et al., 2023). The present study employed Sheorey's equations (3.6) and (3.7) to calculate the in-situ stress in both vertical and horizontal directions, as well as to initialize the in-situ stress gradient with respect to the depth of the working within the model (Sheorey et al., 1989). The next step was to solve the model to get an equilibrated state.

$$\sigma_v = \gamma H \quad \text{(MPa)} \tag{3.6}$$

$$\sigma_h = 2.4 + 0.01H \quad \text{(MPa)} \tag{3.7}$$

In contrast, σ_v stands for vertical stress, σ_h for horizontal stress, γ for the unit weight of rock, and H for the depth of the gallery. The rock unit weight is 0.025 MPa/m, and equation (3.6) is based on the overburden load. The statistical data of observed rock load height for various combinations of dimension and stress conditions are tabulated in Table 3.4.

Table 3.4: Statistical data of observed *RLH* for various dimensions and depths of galleries.

Depth of gallery (m)	**Width of gallery (m)**	**Height of gallery (m)**	***RLH* (m)**		
			Range	**Average**	***SD***
50 m, 100 m, 150 m, 200 m, 250 m, 300 m & 350 m	3.0 m, 4.0 m, 5.0 m	3.0 m, 4.0 m	1.2-2.9	1.98	0.38

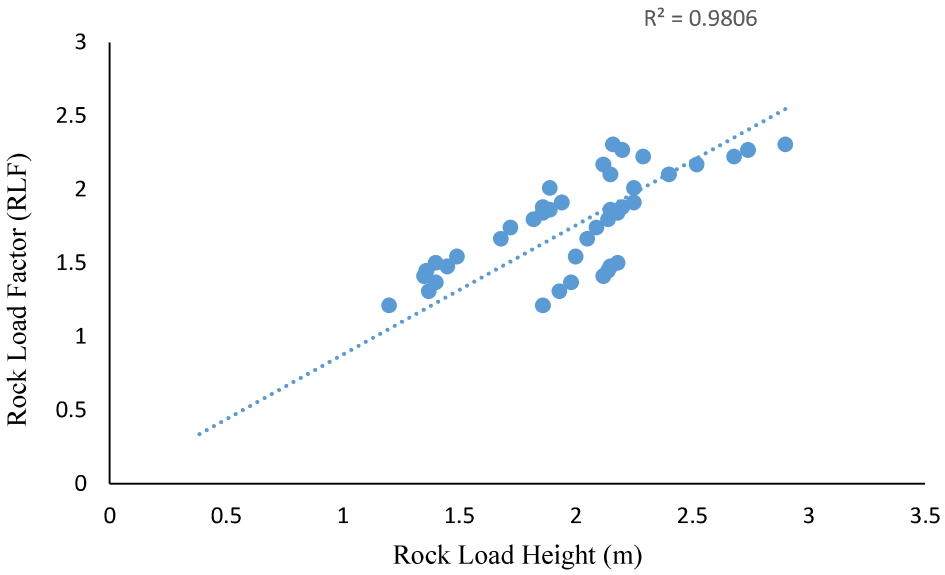

Fig. 3.6: Observed rock load height for various dimensions and depths of the gallery

The effect of depth and gallery dimension on the *CRI* has been represented by the *RLF*. The best-fit equation between observed rock load height and proposed *RLF* has been shown in Fig. 3.6.

Table 3.5: Summary of Regression Analysis

Multiple R	**0.9914876**
R^2	**0.9830477**
Adjusted R^2	**0.9811642**
Standard error	**0.02708**
Observations	**42**

Parameters	Standardized regression coefficient (b*)	Standard error of *b**	Raw regression coefficient (b)	Standard error of *b*	t-stat	P value
Intercept			-0.31348	0.061703	-19.2369	0.000000
Width	0.919580	0.030689	0.84669	0.028256	29.9649	0.000000
Depth	0.370703	0.030689	0.11257	0.009319	12.0795	0.000000
Height	0.456820	0.020459	0.16257	0.009836	18.6965	0.000000

The correlation between Rock load height obtained from numerical method and input variables, width, depth, and height of the gallery, was analyzed using the multiple regression method (Table 3.5). A very strong correlation of rock load height values was found with input variables. Statistical analysis shows that the coefficient of determination (R^2) value is 0.98, which is acceptable for the establishment of multivariate nonlinear equations. The data is said to be statistically significant if the P-value (level of significance %) is less than 0.05. Therefore, as per Table 3.4, input variables width, depth, and height of the gallery are statistically significant for estimation of *RLF*. An empirical equation was developed to estimate the *RLF* for development workings, as shown in equation 3.8. The equation is as follows:

$$RLF = 0.27 \times w^{0.84} \times h^{0.16} \times H^{0.11} \quad (3.8)$$

Whereas, *w* - width of roadway/gallery in m

h- Height of roadway/gallery in m

H - depth of roadway/gallery in m

The suggested adjustment in *CRI* classification, considering the proposed *RLF* equation, is similar to the well-established *CMRI-RMR* adjustment. The rating value for the *RLF* varies from 1 to 2.5 in five equal divisions, while the *RLF* value extends from 1.1 to 2.29. Table 3.6 illustrates the rating system for *RLF*.

Table 3.6: Rating System for *RLF*

RLF	0-1.0	1-1.5	1.5-2.0	2.0-2.5	>2.5
Rating Value R_{CRI_6}	1.0	1.25	1.75	2.25	2.5

3.3.6.1 Stress profile and yielded plastic zone around roadway/gallery

Excavation-induced stress redistribution can result in a pronounced plastic zone that can cause significant financial losses or casualties. As such, plastic zone research has become more and more crucial. (Sun et al., 2021; Zhu et al., 2014). In the plastic zone, the quality of the roof rock deteriorates, which could result in rock collapse and reduced gallery stability (Deng & Liu, 2020). At greater depths, rock typically exhibits notable nonlinear mechanical behavior. The extent of the plastic zone (*PZ*) surrounding underground roads and the redistribution of stress are influenced by the depth and geometrical dimensions (Qiao et al., 2023). Therefore, to illustrate the impact of depth and width on *PZ*, several numerical simulations were conducted using the *H-B* constitutive model. The phase 2D software was used for the analysis of the plastic zone.

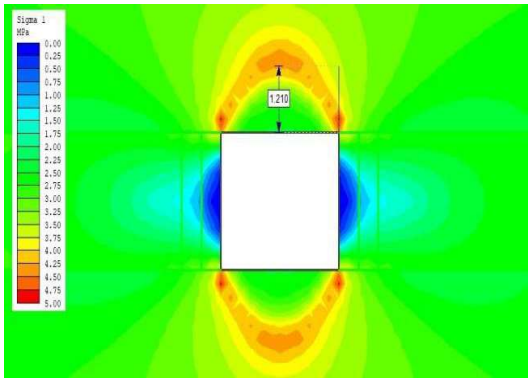

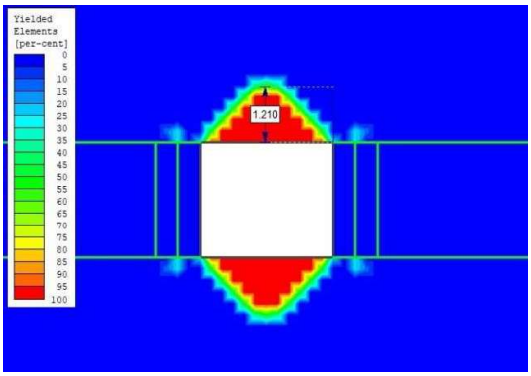

(a) (i) Stress profile for w-3 m & H-50 m (ii) Yield zone view for w-3 m & H-50 m

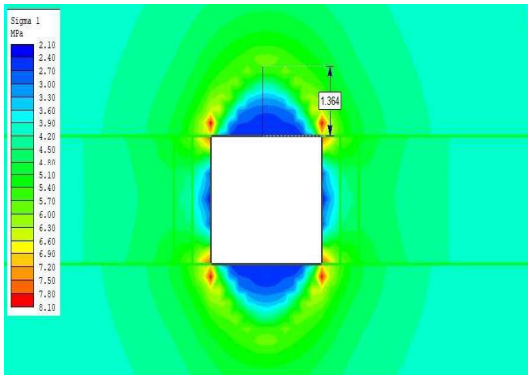

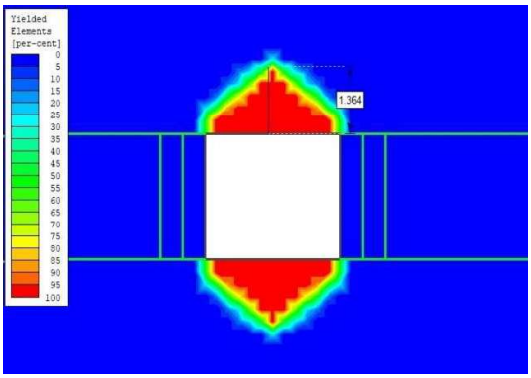

(b) (i) Stress profile for w-3 m & H-150 m (ii) Yield zone view for w-3 m & H-150 m

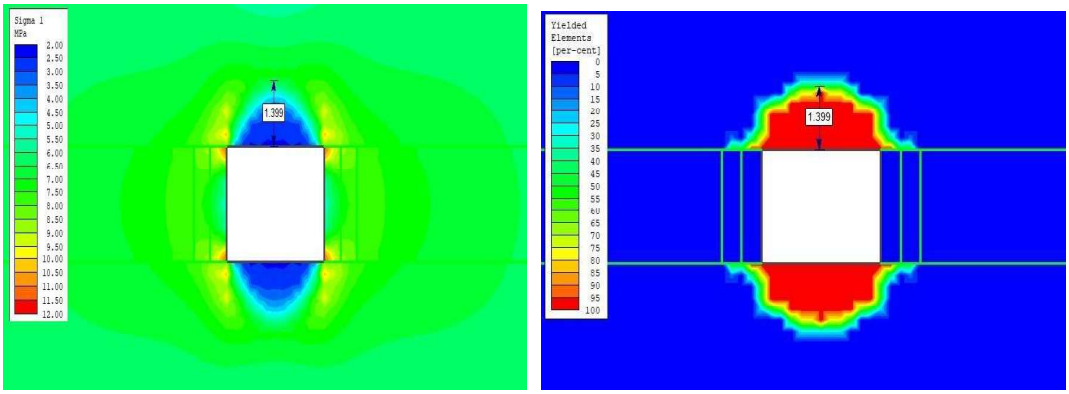

(c) (i) Stress profile for w-3 m & H-250 m (ii) Yield zone view for w-3 m & H-250 m

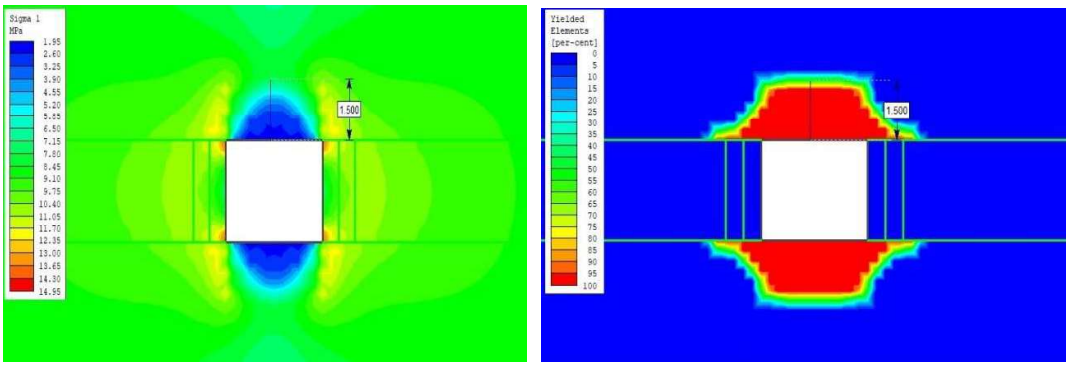

(d) (i) Stress profile for w-3 m & H-350 m (ii) Yield zone view for w-3 m & H-350 m

Fig. 3.7: Stress profile and yield zone height for the width of galleries 3 m and various gallery depths (50 m, 150 m, 250 m, 350 m)

The maximum principal stress redistribution and plastic zone around the 3 m wide gallery for various depths are presented in Fig 3.7. As the depth of the coal gallery increases, the overburden pressure (the weight of the rock above the gallery) also increases. This leads to higher stresses around the gallery. Greater depth results in a larger plastic zone around the gallery. The increased stress can cause more significant deformation and yielding of the rock mass surrounding the gallery. The height of the plastic zone increases with the increasing depth of the gallery. The height of *PZ* is 1.2 m observed for 50 m deep, and it increased up to 1.5 m for the 350 m depth. The shape of the observed plastic zone is a 'V' shape up to the 150 m depth, which means the central part of the excavation yielded more compared to the edge of the excavation. The *PZ* shape

changed to nearly extended 'U' shape after 200 m depth and yielding of elements extended towards the boundary edge of excavation.

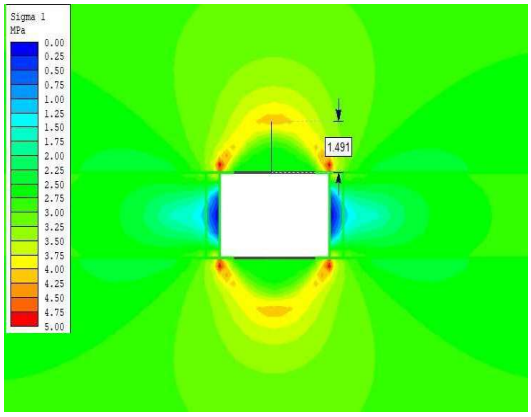

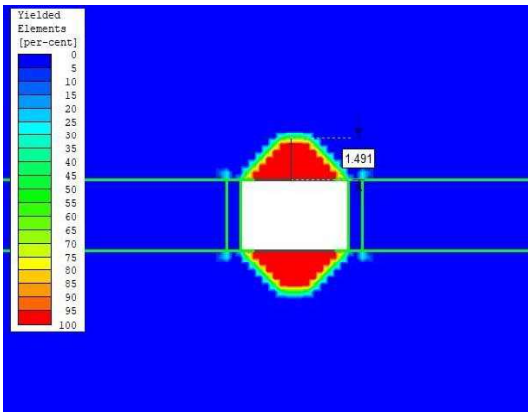

(a) (i) Stress profile for w-4 m & H-50 m (ii) Yield zone view for w-4 m & H-150 m

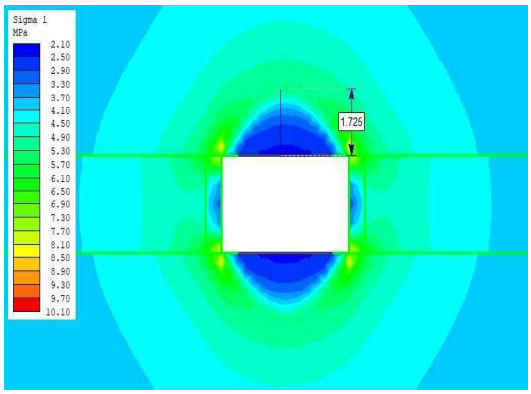

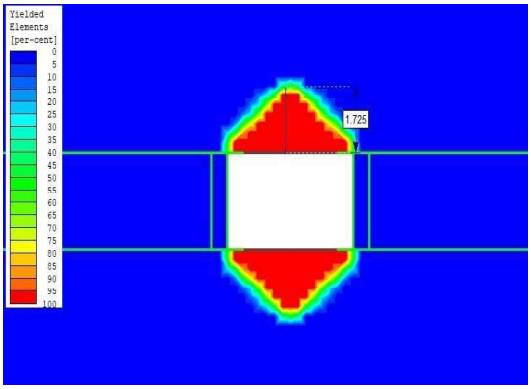

(b) (i) Stress profile for w-4 m & H-150 m (ii) Yield zone view for w-4 m & H-250 m

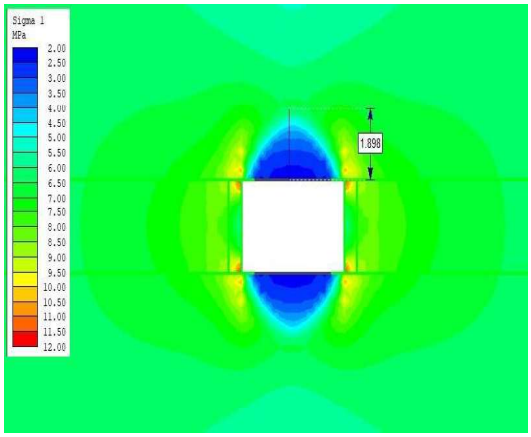

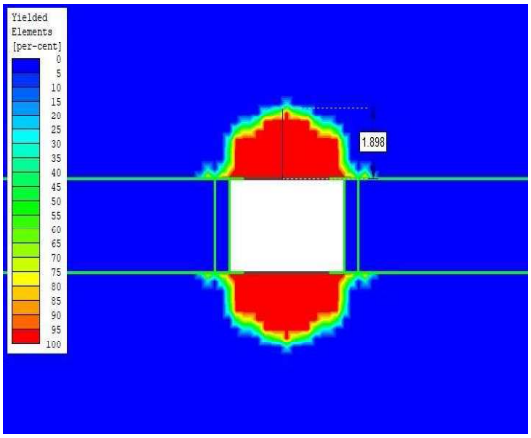

(c) (i) Stress profile for w-4 m & H-250 m (ii) Yield zone view for w-4 m & H-250 m

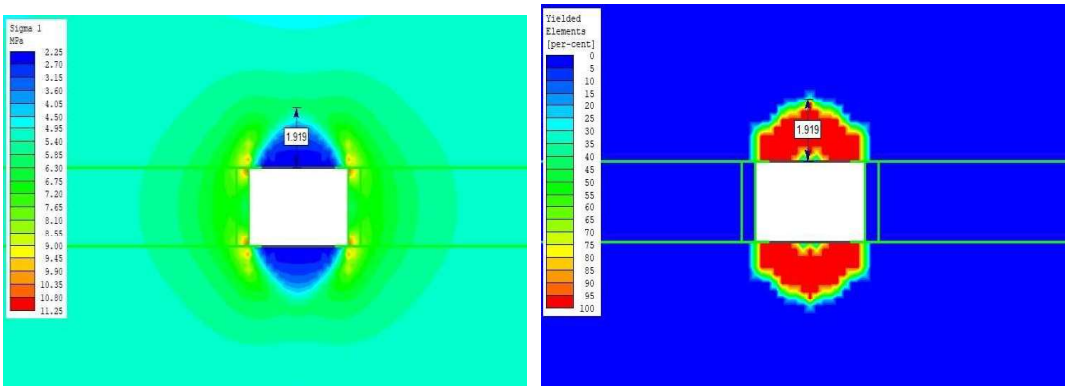

(d) (i) Stress profile for w-4 m & H-350 m (ii) Yield zone view for w-4 m & H-350 m

Fig. 3.8: Stress profile and yield zone height (rock load height) for the width of galleries 4 m and various gallery depths (50 m, 150 m, 250 m, 350 m)

The maximum principal stress redistribution and plastic zone around the 4 m wide gallery for various depths are presented in Fig. 3.8. At greater depths, the rock might experience more extensive yielding and deformation because the stress exceeds the rock's strength over a larger volume. The height of the plastic zone increases with the increasing depth of the gallery. The height of *PZ* is 1.49 m observed for 50 m deep, and it increased up to 1.92 m for the 350 m depth. The shape of the observed plastic zone is a 'V' shape up to the 150 m depth, which means the central part of the excavation yielded more compared to the edge of the excavation. The *PZ* shape changed to nearly an extended 'U' shape after 200 m depth, and yielding of elements extended towards the boundary edge of the excavation.

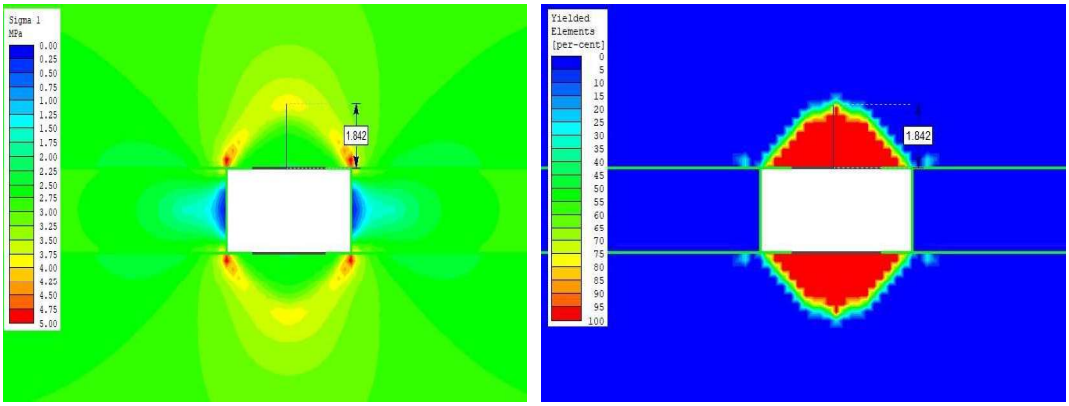

(a) (i) Stress profile for w-5 m & H-50 m (ii) Yield zone view for w-5 m & H-50 m

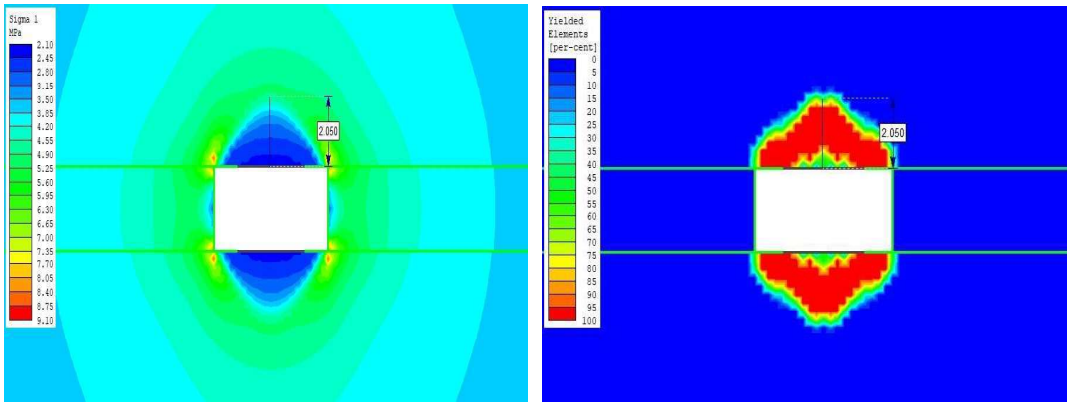

(b) (i) Stress profile for w-5 m & H-150 m (ii) Yield zone view for w-5 m & H-150 m

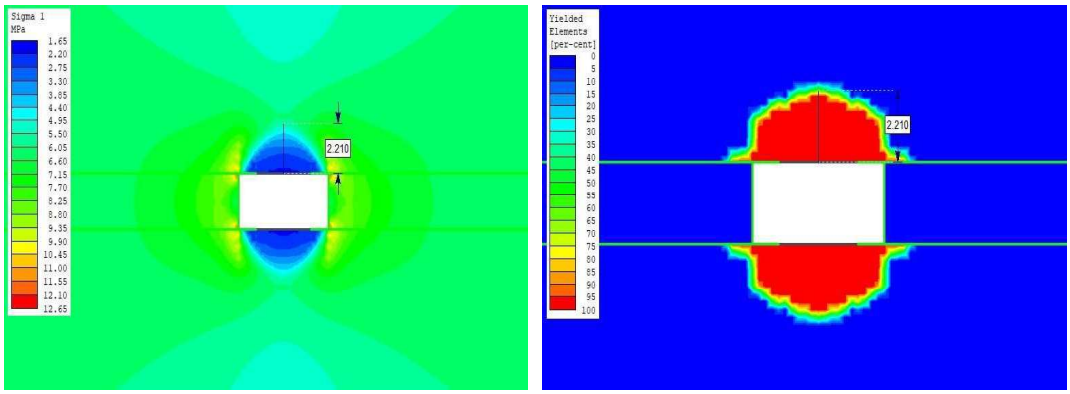

(c) (i) Stress profile for w-5 m & H-250 m (ii) Yield zone view for w-5 m & H-250 m

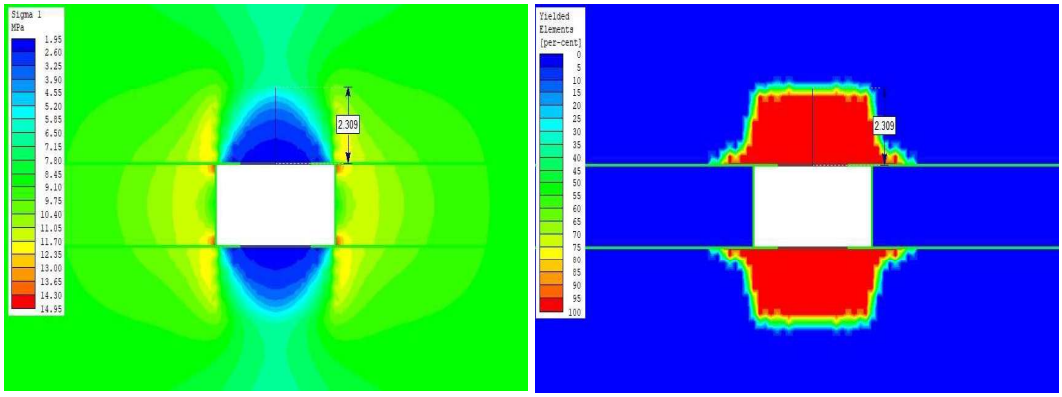

(d) (i) Stress profile for w-5 m & H-350 m (ii) Yield zone view for w-5 m & H-350 m

Fig. 3.9: Stress profile and yield zone height for width of galleries 5 m and various gallery depths (50 m, 100 m, 150 m, 200 m, 250 m, 300 m, 350 m)

The maximum principal stress redistribution and plastic zone around the 5 m wide gallery for various depths are presented in Fig. 3.9. A wider gallery increases the area over which

stress is redistributed, leading to a more extensive plastic zone. The stress concentration around the edges of the gallery becomes more pronounced. The height of the plastic zone increases with the increasing depth of the gallery (Zhongcheng et al., 2016). The height of PZ is 1.84 m observed for 50 m deep, and it increased up to 2.31 m for the 350 m depth. The combined effect of increased depth and width generally leads to a more extensive plastic zone. Deeper and wider galleries face higher stress and deformation, resulting in a more significant yielding zone. The shape of the observed plastic zone is a 'V' shape up to the 150 m depth, which means the central part of the excavation yielded more as compared to the edge of the excavation. The *PZ* shape changed to nearly an extended 'U' shape after 200 m depth, and the yielding of elements extended towards the boundary edge of the excavation.

3.5 Multiple Regression Analysis

The appropriate rating system of the influencing parameters has been evaluated by multiple regression analysis (*MRA*) of the field cases of underground coal mines. The same data set has been chosen for re-analysis of the statistical model of *CRI* with respect to *ST*. The statistical data of the influencing parameters of all 44 cases have been given in Table 3.7.

Table 3.7: Statistical data of the selected 44 Indian coal mines

Parameters	Average value	Stand. Dev.	Range value
LTH (cm)	5.38	2.84	2-15
SF	8.7	3.76	2-17
SDI (%)	94.09	9.37	50-99.5
UCS (MPa)	30.23	12.86	3.5-63
Gw (ml/min.)	362.73	1793.56	1-12000
ST (days)	427.95	594.19	1-1825

Projecting the nature of the relationships between the different input and output variables is the aim of regression analysis. Additionally, it offers the best equation illustrating the relationship between the independent and dependent variables. The result is also predicted using the equation for specific values of the input variables. This study uses *MRA* with ST as the output variable and *LTH*, *SF, SDI, UCS*, and G_w as independent variables.

The *ST* is, by and large, proportional to the *CRI* (eq. 3.9), where the rating of each parameter is correlated with its exponential function. Thus, the multiple regression equation has been framed as follows:

$$ST \propto LTH^a \text{ x } SF^b \text{ x } SDI^c \text{ x } Gw^d \text{ x } UCS^e \quad (3.9)$$

Where LTH^a, SF^b, SDI^c, Gw^d, and UCS^e represent the rating of the respective parameters, i.e. R_{CRI_1}, R_{CRI_2}, R_{CRI_3}, R_{CRI_4}, and R_{CRI_5}.

The main issue is that R^2 magnitude can be significantly impacted by variance in the studied population. Therefore, a high coefficient of determination does not always imply "goodness of fit." Similarly, as the statistic is mostly impacted by changes in the independent variable, there is no assurance that a small R^2 denotes a weak link. Multiple regression analysis has been done for the five independent parameters and one dependent parameter. The independent parameters were *LTH*, *SF*, *SDI*, *UCS* of rock mass, and water conditions. The dependent parameter was recorded as the *ST* in days for all 44 Indian coal mine cases.

The study of 'Nguyen & Nguyen, (2015)' reveals that the *ST* decreases with increasing depth of excavation. The fact that the ground pressure on the underground roadway increases with depth is consistent with this. Thus, the deeper gallery's *ST* is less than that of the shallow gallery. Similarly, increasing the width of the gallery/roadway

reduces the *ST* of the unsupported span. Therefore, the *RLF* has a negative impact on the *CRI* classification. Hence, in *MRA*, the standup time divided by *RLF* and the output value of this friction are considered as dependent variables for all 44 cases. The results of *MRA* are summarised in Table 3.8.

Table 3.8: Multiple regression analysis (MRA) Summary

Multiple R		0.81931244				
R^2		0.67127288				
Adjusted R^2		0.62801931				
Standard error		1.3973				
Observations		44				
Parameters	Standardized regression coefficient (b *)	Standard error of *b**	Raw regression coefficient (b)	Standard error of *b*	t-stat	P value
Intercept			-15.3227	8.046497	-1.90427	0.064467
LTH	0.238301	0.108513	1.1282	0.513736	2.19606	0.034262
SF	-0.448699	0.112199	-2.1488	0.537304	-3.99915	0.000283
SDI	0.223237	0.095497	4.0682	1.740322	2.33764	0.024773
UCS	0.290628	0.098620	1.2989	0.440767	2.94696	0.005458
Gw	-0.083040	0.099806	-0.0829	0.099697	-0.83201	0.410602

While b is employed as a coefficient of independent variables for the computation of the output value, b* represents the contribution or effect of the independent variables (*LTH, SF, SDI, Gw*, and *UCS*) on the dependent variable (*ST*) (Bharati et al., 2022; Uyanık & Güler, 2013). The *MRA* is carried out using the simulation data of 44 coal mine cases in India. The relationship below is demonstrated by the MRA models:

$$\text{Log}(CRI) = -15.32 + 1.128(LTH) - 2.148(SF) + 4.068(SDI) + 1.298(UCS) - 0.0829(Gw) \quad (3.10)$$

3.6 Rating Assessment

The rating range of each parameter has been evaluated by breaking of multiple regression equation (eq. 3.10) into five sub-equations (exponential function), which have been

derived with their coefficients. The values of raw regression coefficients from *MRA* for the respective parameters are as follows:

a = 1.128, b = 2.148, c = 4.068, d = 0.0829, e = 1.298

These constants represent the nature and influence of the parameters on the classification. Figs. 3.10 to 3.14 show the exponential curve of the parameters. The broad range of the parameters, as mentioned in Table 3.9, has also been shown in the curve.

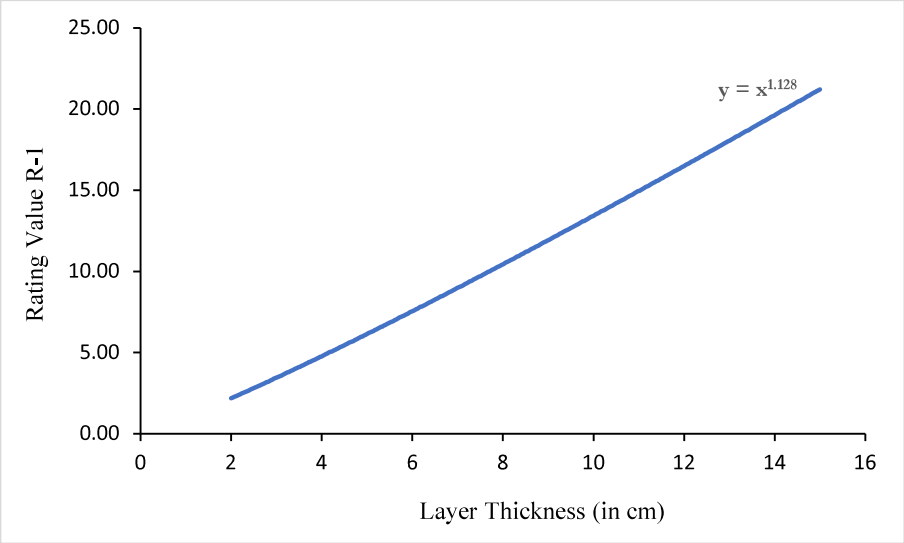

Fig. 3.10: CRI rating scale for *LTH*

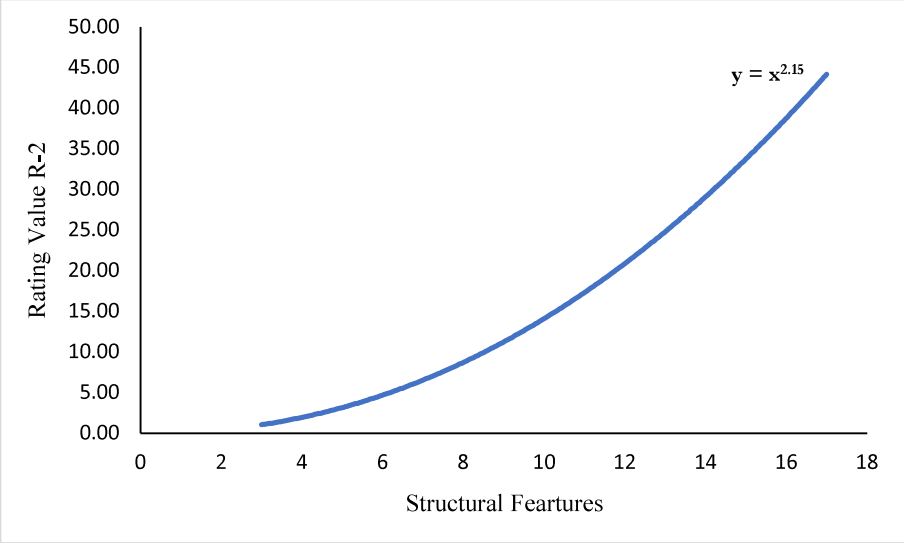

Fig. 3.11: *CRI* rating scale for *SF*

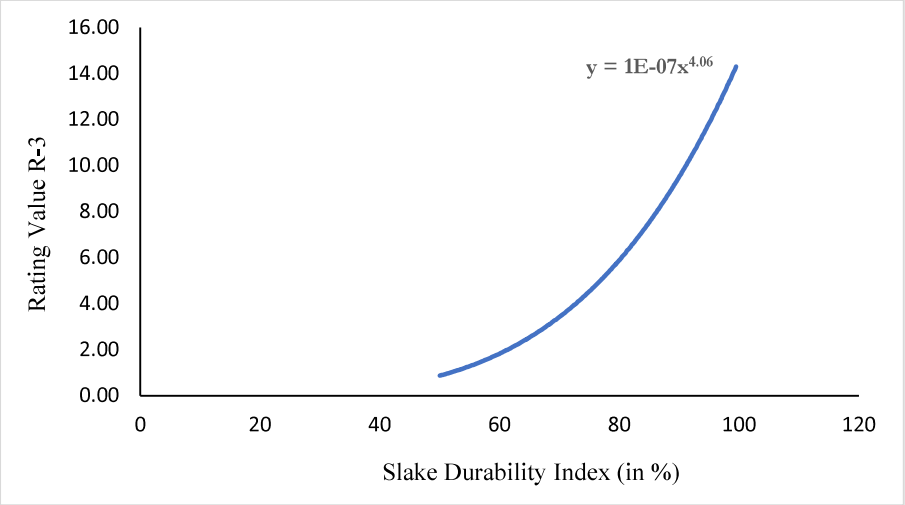

Fig. 3.12: *CRI* rating scale for *SDI*

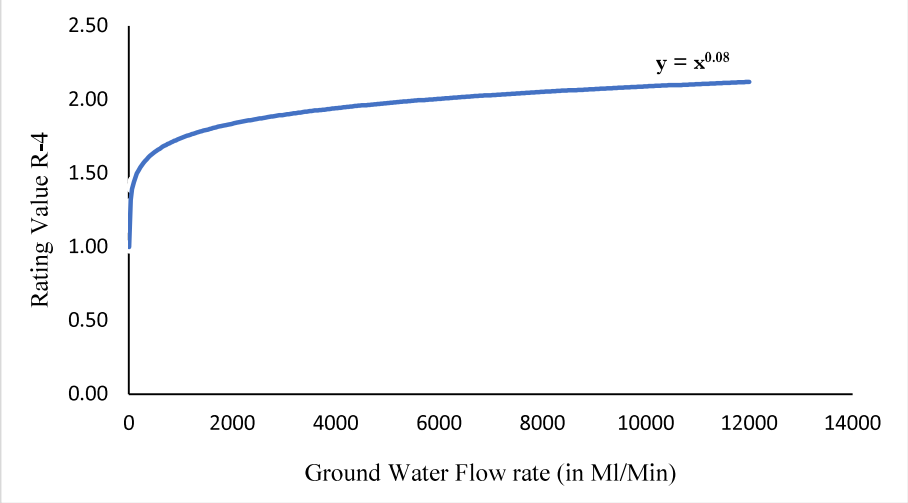

Fig. 3.13: *CRI* rating scale for *Gw*

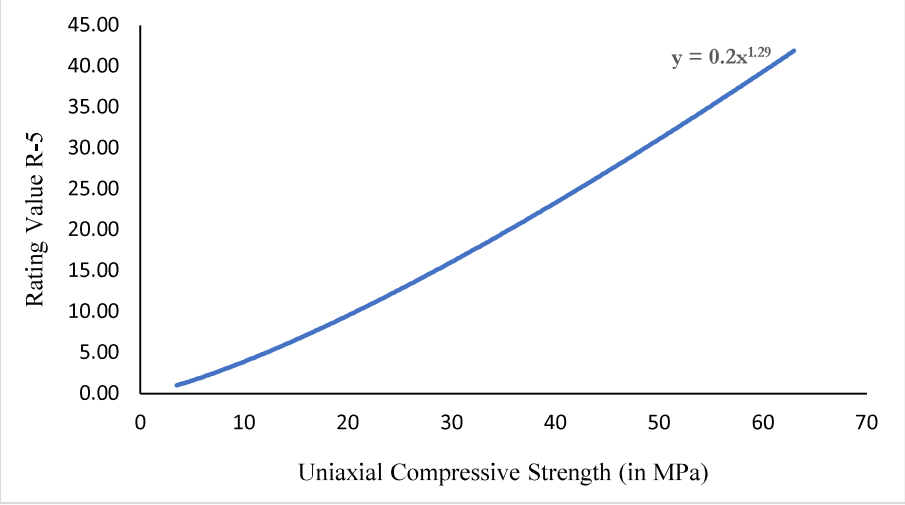

Fig. 3.14: *CRI* rating scale for *UCS*

The rating system has been prepared by considering the regression coefficients of each parameter and plotting the rating range of the actual value of each parameter as shown in Fig. 3.10 to Fig. 3.14. The ratings of each parameter have been distributed among the equation curves by dividing them into five to seven equal divisions within the broad range.

With rating values split into seven divisions ranging from 1 to 25, the *LTH* value is distributed broadly between 0 and 16 cm. For rating ranges from 1 to 30, the structural feature value is distributed between 0 and 18, and rating values are split into six divisions. The equation curve has been split into six divisions, with rating allocation done from 0.2 to 4.5, based on the distribution of the *SDI*, which is roughly 40 to 99. Since the value of *UCS* is distributed between 3 to 70 *MPa*, the rating value is divided into six equal divisions, ranging from 4 to 25. The *Gw* ranges from 0 to more than 10,000 ml/min, and their rating value ranges from 1 to 1.7 in six equal divisions.

Table 3.9 displays the rating system for five rock mass parameters. These have been revised several times to keep them in line with actual observations. To facilitate computations, the positive stability-affecting parameters are *LTH*, slake durability, and *UCS*, and negative stability-affecting parameters as groundwater, *SF*, and *RLF*, whose values increase and worsen the condition of the roadway's roof.

Table 3.9: Rating system for *CRI* classification.

LTH in cm	0-2	2-4	4-6	6-8	8-10	10-12	12-14	>14
Rating value R_{CRI_1}	1	5	8	12.5	16	20	24	27
SF	0-3	3-6	6-9	9-12	12-15	>15		
Rating value R_{CRI_2}	2	4	8	15	25	35		
SDI in %	<40	40-60	60-80	80-90	90-95	>95		
Rating value R_{CRI_3}	0.25	0.5	1.0	1.5	2.5	3.25		
Gws in ml/min.	0-5	5-50	50-250	250-1000	1000-2500	>2500		
Rating value R_{CRI_4}	1	1.5	2.5	3.5	3.75	4.0		
UCS in MPa	0-10	10-20	20-30	30-40	40-50	>50		
Rating value R_{CRI_5}	1	4	7	11	15	20		

Therefore, as shown in equation 3.2, the positive influencing parameter rating was the numerator, and the negative influencing parameter's rating was put in the denominator in the calculation of the *CRI* value of roof rock.

3.7 Result and Discussion

3.7.1 Coal Roof Rock Class Categorization for proposed *CRI* classification

Based on *ST*, the proposed *CRI* classification range has been divided into seven classes: extremely poor (less than one week), very poor (less than one month), poor [one to three months], fair [three to seven months], good [seven to twenty months or less than 1.5 years), and very good [> twenty months or less than 5 years), and extremely good (> five years). The extremely weak and extremely strong class coal roof rock are very rarely observed in the field. The selected data has not fallen in these two classes, so it is not shown in Fig. 3.15. The class system and the *ST* range are displayed in Fig. 3.15. Black dotted lines represent the upper and lower bounds of the scattered data for each of the 44 cases, while dark orange lines represent the average value.

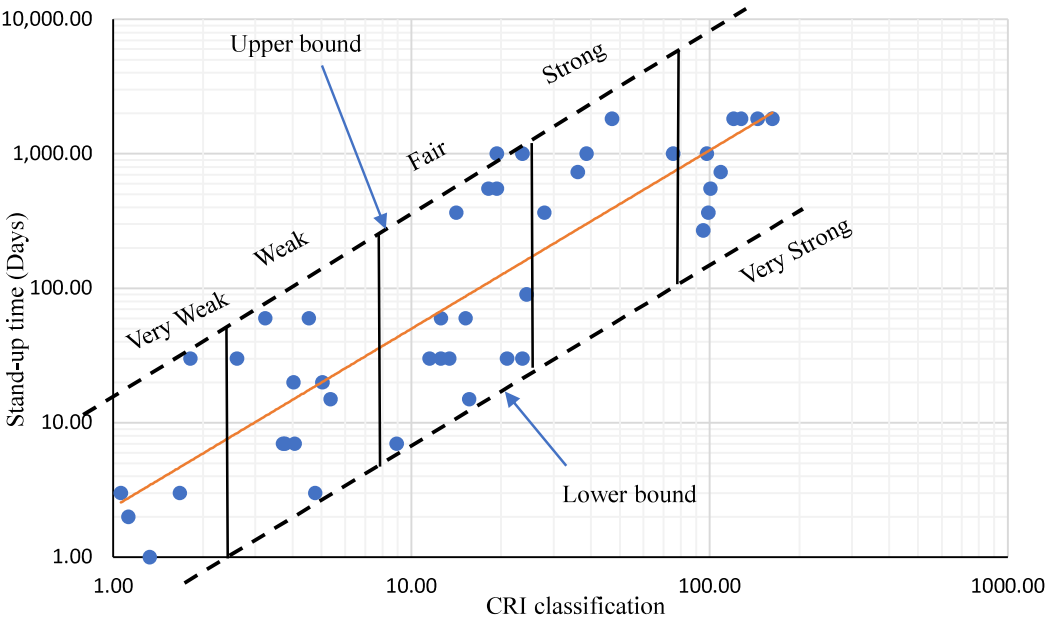

Fig. 3.15: *CRI* classification

Table 3.10 summarizes the statistical analysis of the data set, which was completed for each of the classes based on the *ST* and *CRI* value.

Table 3.10: Classification of coal roof rock based on *CRI* values and *ST*

Coal Roof Description	*CRI* Value	*ST* (days)	
		Average	Standard deviation
Extremely weak	0.001-0.1	0-1	-
Very weak	0.1-2.5	5	7.4
weak	2.5-7.5	30	21.47
Fair	7.5-25	323	363.5
Strong	25-75	1093	563.7
Very strong	75-400	1278	751.8
Extremely Strong	400-1000	>1825	-

3.7.2 Correlation with *ST*

Fig. 3.16 displays the scattered data between *ST* and *CRI* for each of the 44 cases plotted on a logarithmic scale. The plotting of the best-fit linear trend is also included. The *ST* of a gallery increases with increasing *CRI* values. Estimating the *ST* of an underground coal mine is a valuable tool in determining the necessary level of support. It will help the field engineers to design the excavation cycle and estimation of cut-out distance without support for a stable coal gallery.

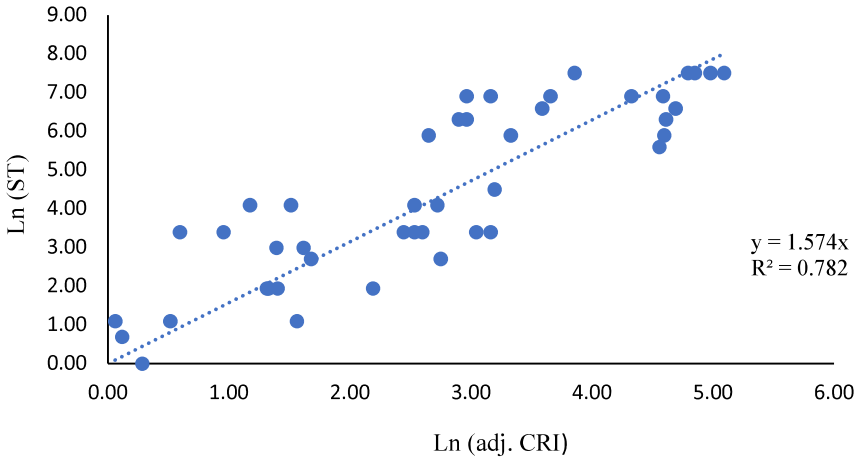

Fig. 3.16: A graphical plot between adj. *CRI* and *ST*

The following linear logarithmic formulation has been proposed:

$$Ln\ (ST) = 1.5746\ Ln\ (CRI) \tag{3.11}$$

The coefficient of determination (R^2) has been obtained as 0.78. As shown in Fig. 3.16, the *CRI* classification has around a 29 percent increase coefficient of determination as compared to the *CMRI-RMR* classification.

3.7.3 Comparison between *CRI* classification and *CMRI-RMR* classification

As discussed earlier, *CMRI-RMR* showed a poor correlation with *ST* for the short-term stable cases (≤30 days). Therefore, a correlation graph has been plotted for both the *CMRI-RMR* and proposed *CRI* classification system vis-à-vis *ST* in Figs 3.17 and 3.18, respectively. Fig. 3.17 shows the scattered data plot for the *CMRI-RMR* classification. It has observed a very low R^2 value concerning *ST*, which is about 0.48. The *CRI* value ranges from 0.001 to 1000. It has a good R^2 value, which is 0.78, and the graph plot has also shown conformity with the best fit line in Fig. 3.18.

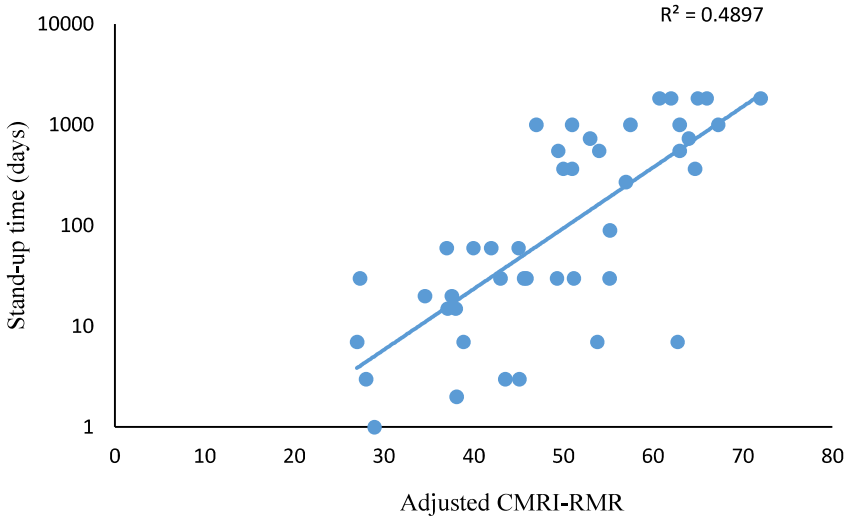

Fig. 3.17: Correlation between recorded *ST* and Adj. *RMR*

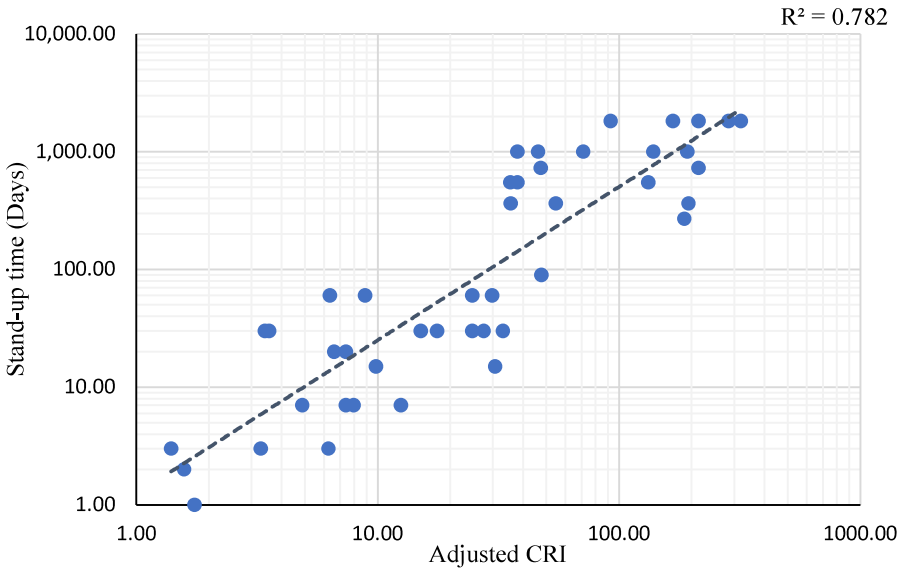

Fig. 3.18: Correlation between recorded *ST* and adjusted *CRI*

The comparison in Table 3.11 highlights that the proposed CRI addresses several limitations of the *CMRI-RMR* by incorporating a multiplicative rating approach and integrating span–stress adjustments through the *RLF* derived from numerical modelling. These enhancements result in a stronger correlation with stand-up time (R^2 = 0.67 compared to = 0.45) and reduced prediction error, thereby improving the reliability of roof stability predictions. Furthermore, the *CRI's* empirical linkage to Hoek–Brown parameters enables direct application in numerical modelling, facilitating more realistic and site-specific support design for underground coal mines.

Table 3.11: Comparison between *CMRI-RMR* and *CRI*

Feature / Metric	*CMRI-RMR*	CRI (Proposed)	Improvement / Advantage
Purpose	Developed for estimating rock load and support design in Indian coal mines	Designed to estimate stand-up time and support design in Indian coal mines, and link to Hoek–Brown strength parameters	Broader applicability and numerical modelling integration
Rating Method	Additive	Multiplicative	Multiplicative system penalises weak parameters more realistically
Span/Stress Adjustment	Not explicitly included	Adjusted via Rock Load Factor (*RLF*) from numerical modelling	Accounts for gallery span and in-situ stress
Correlation with Stand-Up Time (R^2)	~0.45 (dataset of 44 cases)	~0.67 (same dataset)	Improved predictive accuracy
Link to Hoek–Brown Parameters	Not available	Empirical equations developed for m, s, and a from CRI	Direct integration into numerical modelling
Field Validation	Moderate	Stronger agreement with independent cases	Improved reliability for design decisions

3.7.4 Correlation among *CMRI-RMR* and the *CRI* Classification

Regression analysis has been used to establish a statistical correlation between *CRI* classification and *RMR* classification. The scattered data's exponential best-fit curve is displayed in Fig. 3.19. The coefficient of determination between the *CRI* and *CMRI-RMR* data sets is 0.78, which is deemed a good correlation based on the results.

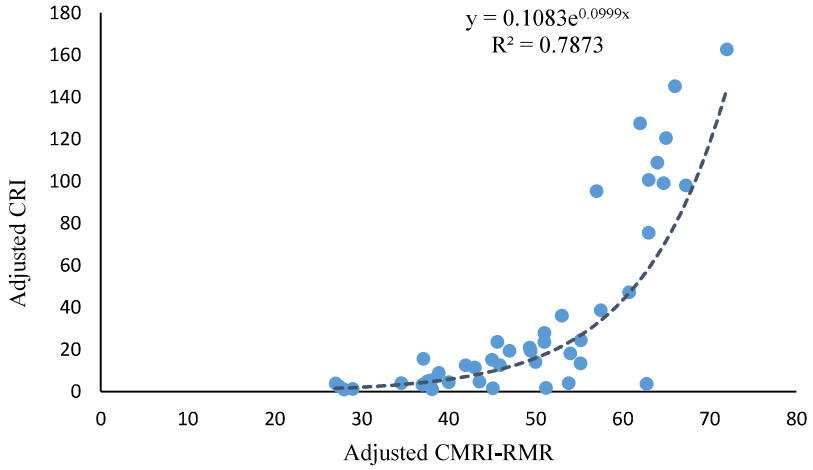

Fig. 3.19: Correlation between *CMRI-RMR* classification and *CRI* classification

The following exponential relationship has been developed:

$$CRI = 0.1083e^{0.0999\ RMR} \quad (3.12)$$

$$R^2 = 0.7873$$

3.8 Validation through Indian coal mine failed/stable cases

Four Indian coal mine cases have been considered for the validation of the study. Details of *CRI* classification parameters and their rating values are given in Table 3.11. The *CRI* value and *ST* for all cases have been determined by the suggested formulation (Eq 3.2 and Eq. 3.7, respectively). As per the study of Paul et al. (2023), and Paul et al. (2012), Pandavpara Mine is a stable case, and Piparia Mine and Monnet Ispat Mine, Seam II are unstable cases. This study also shows that the *CRI* value of Pandavpara Mine is 74.28, which comes under the strong category of rock, and the projected *ST* is more than 880 days, which indicates stable roof rock. The calculated *CRI* values for Piparia Mine and Monnet Ispat Mine, Seam II, are 2 and 4.57, which come under the poor category of roof rock. The projected *ST* for both cases also shows unstable behaviour of the roof rock, even with roof support as per the suggested equation 7. The Shyampur Colliery has a *CRI* value of 130, which comes under the very strong category of rock, and the projected *ST* for this case is more than five years, which indicates the stable nature of the roof rock. It has also been observed in the field that galleries of inclines 5 & 6 of Shyampur Colliery were stable without any support for more than five years.

Nowadays, underground galleries are supported just after the excavation stage. Therefore, it is difficult to measure the actual *ST* of unstable cases in the condition of no support. As per the author's knowledge, similar literature is not been available. However, two unstable cases have been picked from A. Paul et al. (2023). Which failed even after the support of as per the *RMR* guideline. It is expected that these two cases have a very

short *ST* in the condition of no support, which is also evident from this study. So, this study shows good agreement in the classification of roof rock and an average prediction of the *ST* of a coal mine.

Table 3.12: Four Indian coal mine cases considered for validation.

Mine name & *Rating Value*	***LTH* (cm)**	***SF***	***SDI* (%)**	***UCS* (MPa)**	**Ground water**	***RLF***	**Adj. *CRI* value**	**Stable / Unstable**	***ST* (Days) By Eq. 3.7**
Pandavpara Mine	14.9	6	93	28.78	Moist	1.80	74.28	Stable	880.06
Rating value	16	4	2.5	13	1	1.75			
Piparia Mine	4.53	11	83.46	15.08	Moist	1.77	2	Un-stable	2.97
Rating value	5	15	1.5	7	1	1.75			
Shyampur Colliery	13.4	6	98.6	79.2	Moist	1.76	130	Stable	2121.75
Rating value	16	8	3.25	35	1	1.75			
Monnet Ispat Mine, Seam III	7	9	88.7	24	225 ml/L	1.78	4.57	Un-stable	10.91
Rating value	7.5	15	1.5	13	1.2	1.75			

3.9 Concluding Remarks

The evaluation of the roof's rock-mass characterization is crucial for determining the necessary roof support. The *CRI*, a rock-mass classification system for coal roof rocks, was developed using the statistical analysis of forty-four Indian coal field cases. The greater depth tends to increase the extent of the plastic zone due to higher overburden pressure, while a wider gallery usually results in a larger plastic zone due to increased stress redistribution. Proper engineering design must account for these factors to maintain stability and safety in underground mining operations. Therefore, the combined effect of the depth and width of the gallery was introduced by the *RLF* in the present classification system. The suggested classification scheme is based on multiplying the ratings of the six

influencing factors—*Gw, LTH*, weatherability, *SF, UCS* of roof strata, and *RLF*. The *CRI* ranges from 0.001 to 1000. Seven classes have been identified based on the *CRI*: Extremely Weak (*CRI*: 0.001 – 0.1), Very Weak (*CRI*: 0.1 – 2.5), Weak (*CRI*: 2.5 – 7.5), Fair (*CRI*: 7.5 - 25), Strong (CRI: 25 - 4), Very Strong (CRI: 75 - 400), and extremely strong (*CRI*: exceeding 400). While *LTH*, SDI, and *UCS* of roof strata show a positive influence on the *CRI*, as well as *SF, Gw*, and *RLF* show a negative influence on CRI. When weatherability is less than 95%, Gw must be taken into account. The suggested *CRI* value and the *ST* had a respectable correlation, according to a statistical analysis of the large range of roof rock quality.

.